Materials Horizons

ROYAL SOCIETY OF CHEMISTRY

COMMUNICATION

View Article Online
View Journal | View Issue

Cite this: *Mater. Horiz.*, 2023, 10, 2554

Received 14th February 2023,
Accepted 11th April 2023

DOI: 10.1039/d3mh00218g

rsc.li/materials-horizons

A cyclic brush zwitterionic polymer based pH-responsive nanocarrier-mediated dual drug delivery system with lubrication maintenance for osteoarthritis treatment†

Miao Zhang,[a] Xu Peng,[b] Yuan Ding,[a] Xiang Ke,[a] Kai Ren,[a] Qiangwei Xin,[a] Meng Qin,[a] Jing Xie *[a] and Jianshu Li *[acd]

Enhanced joint synergistic lubrication combined with anti-inflammatory therapy is an effective strategy to delay the progression of early osteoarthritis (OA) but has been rarely reported. The hydration lubrication of zwitterions and inherent super-lubrication properties of the cyclic brush, as well as the enhancement of the steric stability of the cyclic topology, can effectively improve the drug loading and utilization; herein we report a pH-responsive cyclic brush zwitterionic polymer (CB) with SBMA and DMAEMA as brushes and a cyclic polymer (c-P(HEMA)) as the core template, possessing a low coefficient of friction (0.017). After loading with hydrophobic curcumin and hydrophilic loxoprofen sodium it demonstrates high drug-loading efficiency. *In vitro* and *in vivo* experiments confirmed the triple function of the CB on superlubrication, sequence controlled release and anti-inflammatory effects demonstrated by Micro CT, histological analysis and qRT-PCR. Overall, the CB is a promising long-acting lubricating therapeutic agent, with potential for OA treatment or other diseases.

New concepts

To date, research on cyclic brush zwitterionic polymers remains blank, and little is known about their biological properties. In this study, for the first time we synthesized a series of stable cyclic brush zwitterion polymers as a synergistic lubricant. Owing to the enhanced steric stability coupled to the inherent absence of chain ends using a cyclic brush, as well as the hydration lubrication of the zwitterionic polymer, the self-assembled cyclic brush exhibits a highly synergetic lubrication effect. In addition, the unique properties of the cyclic brush zwitterionic polymer enable the co-loading of hydrophilic and hydrophobic anti-inflammatory drugs with higher drug loading efficiency compared to the polymer micelle morphologies reported. For the SD rats with early osteoarthritis, the injection of the cyclic brush zwitterionic polymer on the articular cavity has superlubrication, sequence-controlled release and anti-inflammatory effects, thus can effectively treat osteoarthritis. We are excited about this discovery, which contributes to a more comprehensive and in-depth understanding of the biological properties of cyclic brush zwitterionic polymers and has guiding implications for the design of smart biomedical materials.

Introduction

Osteoarthritis (OA) is a chronic joint disease characterized by degeneration, destruction of articular cartilage and hyperplasia of bone, mainly manifested by cartilage injury, subchondral osteosclerosis, synovial inflammation and osteophyte hyperplasia at the joint margin. Moreover, OA is associated with increased mechanical friction of the joints, and its pathological process is irreversible.[1,2] Currently, there are generally two effective OA interventions: (1) enhancing the lubricating properties of the joint or promoting cartilage repair; and (2) drug therapy, but due to the lack of blood vessels in the articular cartilage, the absorption rate of oral anti-inflammatory drugs is low, and frequent oral or intravenous administration may cause drug resistance, overdose, and gastrointestinal problems.[3–6] Therefore, the development of a synergistic treatment modality that can enhance lubrication and precise specific drug delivery is highly desirable for OA patients.

In recent decades, cyclic polymers have received considerable attention due to their endless chain topology-associated unique properties.[7–9] From the perspective of structural biomimetics, various bottle brush and cyclic brush polymers were prepared by simulating the brush-like structure of a natural glycoprotein lubricant (LUB).[10–12] Specifically, the smaller hydrodynamic radius of the cyclic polymer side chains and the inherent absence of cyclic chain ends result in a denser and more lubricated brush on the cartilage surface compared to the linear structure, exhibiting better lubrication properties and

[a] College of Polymer Science and Engineering, State Key Laboratory of Polymer Materials Engineering, Sichuan University, Chengdu 610065, P. R. China. E-mail: xiej@scu.edu.cn, jianshu_li@scu.edu.cn
[b] Experimental and Research Animal Institute, Sichuan University, Chengdu 610065, P. R. China
[c] State Key Laboratory of Oral Diseases, West China Hospital of Stomatology, Sichuan University, Chengdu 610041, P. R. China
[d] Med-X Center for Materials, Sichuan University, Chengdu 610041, P. R. China

† Electronic supplementary information (ESI) available. See DOI: https://doi.org/10.1039/d3mh00218g

biological activity.[13–15] The cyclic brush can not only be an alternative for natural bio-lubricants, but also its enhanced steric stability can effectively improve the drug loading and drug utilization and prolong circulation time. Based on the hydration lubrication mechanism proposed by Klein *et al.*, zwitterionic polymers demonstrate excellent lubrication properties owing to their super high hydrophilicity. Among them, [2-(methacryloyloxy)ethyl]dimethyl-(3-sulfopropyl) (SBMA) is widely used due to its super lubricating performance.[16–18] However, until today, cyclic brush zwitterionic polymer materials have been rarely reported. Therefore, based on the inherent lubrication characteristics of zwitterionic polymers and the enhanced spatial stability of a cyclic topology, the elegant combination of the two to form a cyclic brush zwitterionic lubricant is very promising to have synergistic lubrication effects and restore lubricating properties on the articular cartilage in OA.

So far, the most widely used joint injection materials in the clinical stage include hyaluronic acid (HA),[19] corticosteroids (GC),[20,21] platelet-rich plasma (PRP)[22] and stem cell therapy.[23] Although it has been reported that diclofenac sodium (DS),[1,24] curcumin (Cur),[25,26] loxoprofen (LXP),[27] *etc.* can effectively reduce the inflammatory response and oxidative stress levels in OA model rats. However, single-drug therapy is characterized by low loading content, short residence time and single efficacy, which not only fails to treat patients, but also leads to drug-resistant and drug dependence, forming a vicious cycle.[28,29] To date, no single therapy has been shown to improve disease progression in the long term, indicating a great clinical need for novel OA drug delivery carriers or regenerative therapies. Therefore, the dual drug sequence self-release system is highly desirable to achieve satisfactory effect in OA treatment.[30,31] In addition, the bioavailability of drugs is often limited by special biological structures, such as lack of blood vessels, nerves, *etc.*[32,33] In cartilage, the dense structure of cartilage matrix and high density of negative charges also hinder drug penetration.[34,35] Given the complexity and variability of the physiological environment *in vivo*, it remains challenging to design a drug delivery system that is sensitive to changes in the metabolic state *in vivo*, especially the controlled-release system that is sensitive to the low pH with efficient drug delivery in the ideal location of OA.[36,37] In view of the negatively charged properties of cartilage matrix, there have been relevant reports confirming that the modification of drugs by positively charged nanoparticles can overcome the obstacle of drugs with difficulty in penetrating cartilage and effectively improve the utilization of drugs.[38–40] The pH responsive cationic *N*,*N*-dimethylaminoethyl methacrylate (DMAEMA) can not only effectively overcome the dense structural obstacles and negatively charged cartilage, penetrate the cartilage matrix, but also closely bind hydrophilic anti-inflammatory drugs through electrostatic interaction and trigger the controllable release of drugs in joint inflammation sites, is widely used as a carrier for drug delivery in OA treatment.[41–43]

Based on the above-mentioned microstructural and biofunctional alterations of OA, as well as the blank of the synthesis of cyclic brush zwitterionic polymers so far, a superlubricated cyclic brush zwitterionic polymer (CB) was designed for the first time, as shown in Scheme 1. Specifically, we statistically copolymerize SBMA and DMAEMA *via* a ''one-pot'' atom transfer radical polymerization (ATRP) using poly-2-hydroxyethyl methacrylate (*c*-p(HEMA)) as a core template to prepare (*c*b-P(HEMA-*g*-P(DMAEMA-*st*-SBMA)), CB). Furthermore, combined with the enhanced stability of the cyclic topology and the electrostatic interaction of the cationic DMAEMA, the hydrophobic drug Cur and the negatively charged hydrophilic drug LXP can be well loaded. The CB not only realized the dual drug loading and increased the total drug loading, but also significantly showed satisfactory specific drug release and effective delivery to cartilage at the site of joint inflammation attributed to the positive charge under acidic conditions. Tribological experiments showed that the CB had significantly enhanced lubrication (COF $\sim$ 0.017); *in vitro* drug release experiments showed that the dual drug delivery system had pH-responsive long-term sequence controlled release behavior (including early and rapid release of hydrophilic drugs, slow and long-acting release of hydrophobic drugs). Furthermore, *in vitro* cell experiments demonstrated that CB showed good biocompatibility and effectively alleviated chondrocyte degeneration stimulated by inflammation and oxidative stress. Micro CT, histological analysis and qRT-PCR validated the dual lubricating and anti-inflammatory effects of CB in the OA rat model. As we have shown, our first developed cyclic brush zwitterionic polymer-based pH-responsive nanocarrier-mediated dual drug delivery system integrated superlubricated properties, improved drug utilization by high drug loading, specific short-term and long-term release and high-efficiency anti-inflammatory activity. It is a promising novel lubricating and anti-inflammatory therapeutic agent, which is expected to be a potential candidate drug delivery system for the treatment of early OA.

Results and discussion

Syntheses and characterizations of cyclic brush (CB) and bottle brush (BB) zwitterionic polymers

The synthetic routes of cyclic brush (*c*b-P(HEMA-*g*-P(DMAEMA-*st*-SBMA)), CB) and bottle brush (*bb*-P(HEMA-*g*-P(DMAEMA-*st*-SBMA)), BB) zwitterionic polymers are shown in Scheme 1a, b and Scheme S1 (ESI†). The compositions of the four types of cyclic brush polymers are identical and synthesized by atom transfer radical polymerization (ATRP) and copper-catalyzed azide–alkyne cycloaddition (CuAAC) polymerization. First, we synthesized linear precursors (*l*-P(HEMA)$_{50}$-Br), cyclic polymer templates (c-P(HEMA)$_{50}$), as well as linear and cyclic macroinitiators (*l*-P(HEMA-Br)$_{50}$ and *c*-P(HEMA-Br)$_{50}$) through ATRP, intrachain click cyclization, and substitution reactions using propargyl 2-bromoisobutyrate as the initiator. Then, a pH-responsive cyclic brush zwitterionic polymer was meticulously synthesized *via* ''one-pot'' ATRP of zwitterionic SBMA and pH-responsive DMAEMA. Furthermore, by adjusting the feeding ratio of SBMA to DMAEMA, four kinds of cyclic brush polymers (CB1, CB2, CB3 and CB4) with different degrees of polymerization were obtained, respectively. The bottle brush BB analogue was synthesized in the same steps as the CB except that

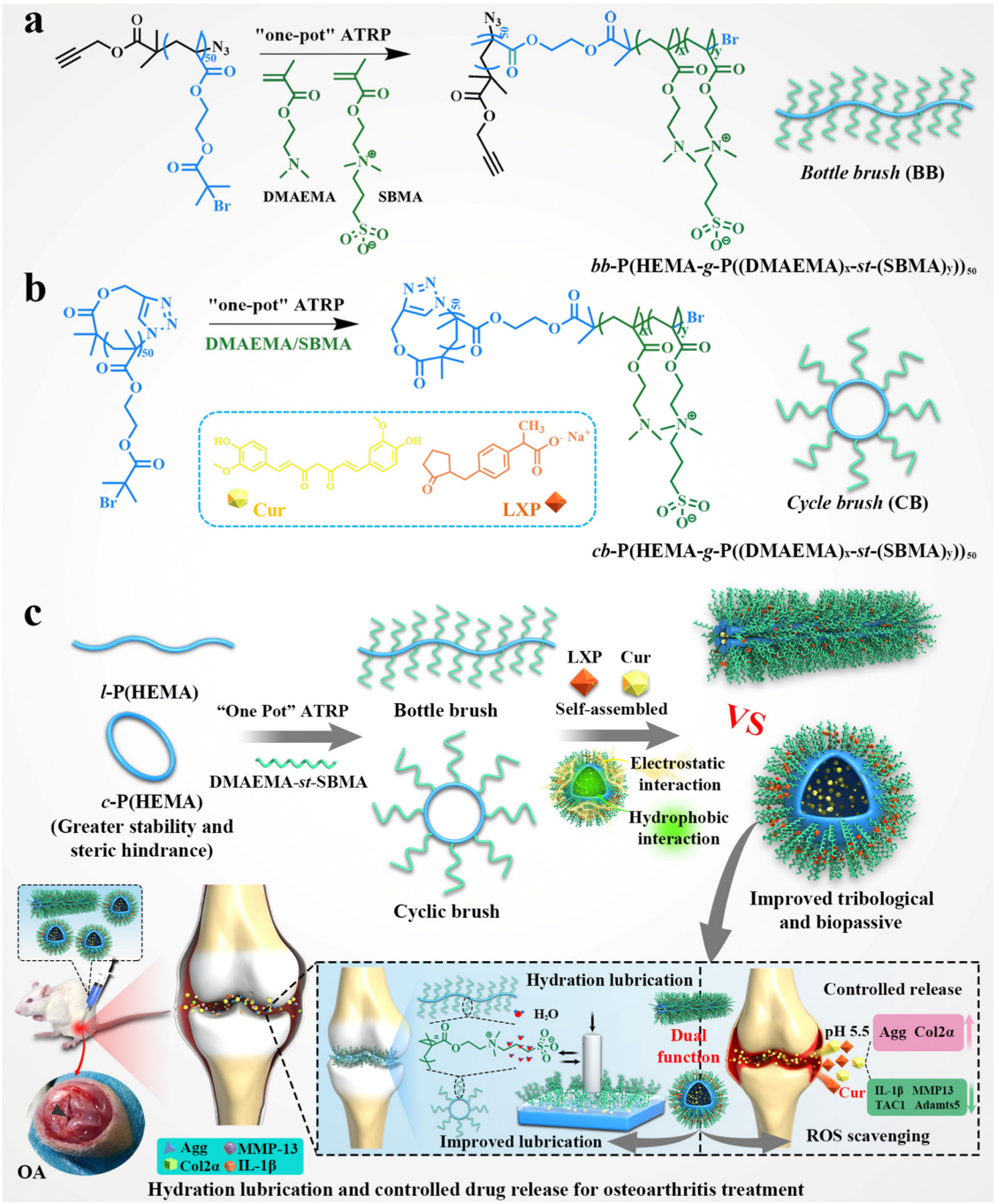

Scheme 1 Synthesis route of (a) bottle brush (BB) and (b) cyclic brush (CB). (c) Schematic illustration of the formation and mechanism of a pH-responsive superlubricated dual-drug cyclic brush zwitterionic polymer with high drug loading for effective treatment of OA.

(l-P(HEMA-Br)$_{50}$) was used as the macroinitiator in the last step. Both cyclic brush and bottle brush polymers possess good water solubility. The polymerization parameters and molecular weight (M_W) of CBs and BB are summarized in Fig. 1a.

The detailed characterization of the intermediate and final products of the four types of CBs and BB can be found in Fig. S1–S13 (ESI†). l-P(HEMA)$_{50}$-Br and c-P(HEMA)$_{50}$ were prepared by ATRP and intrachain click cyclization according to our previous study.[44] The degree of polymerization (DP) of the P(HEMA) was calculated to be ~50 by ^{1}H NMR spectra (Fig. S2, ESI†). Thanks to the controlled molecular weight and polymer composition of ATRP, each step of the polymer product showed a unimodal narrow distribution (Table S3, ESI†). Successful cyclization was evidenced by SEC-MALLS: the c-P(HEMA)$_{50}$ SEC elution profile demonstrates discernible right-shift toward longer retention time (lower M_W) compared to linear precursors (Fig. 1b). Moreover, the disappearance of ethylene protons at 4.65 ppm in the ^{1}H NMR spectra (Fig. S3, ESI†), as

(a)

Polymer composition	Sample	Monomers feed ratio of DMAEMA/SBMA	DP of PDMAEMA	DP of PSBMA	Reaction Time (h)	Molecular Weight (KDa)
cb-P(HEMA-*g*-P(DMAEMA-*st*-SBMA))$_{50}$	CB1	0.67:1	30	45	3	871
cb-P(HEMA-*g*-P(DMAEMA-*st*-SBMA))$_{50}$	CB2	0.83:1	45	45	3	989
cb-P(HEMA-*g*-P(DMAEMA-*st*-SBMA))$_{50}$	CB3	1.33:1	60	45	3	1107
cb-P(HEMA-*g*-P(DMAEMA-*st*-SBMA))$_{50}$	CB4	1.43:1	80	45	3	1204
bb-P(HEMA-*g*-P(DMAEMA-*st*-SBMA))$_{50}$	BB	1.33:1	60	45	3	1107

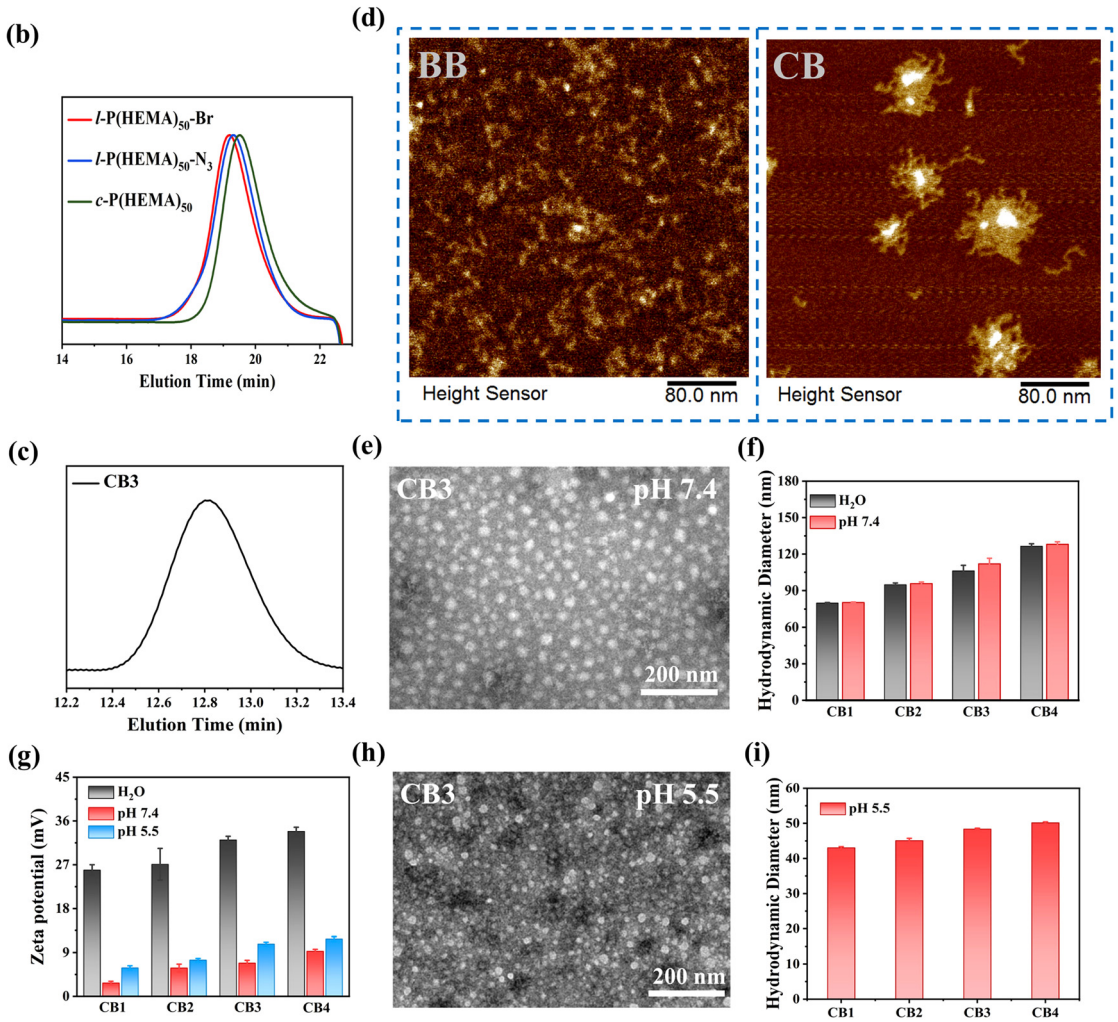

Fig. 1 (a) Summary of molecular weight and DP of all the synthesized CBs and BB polymers. (b) SEC curves of *l*-P(HEMA)$_{50}$-Br, *l*-P(HEMA)$_{50}$-N$_3$ and *c*-P(HEMA)$_{50}$ using DMF as an eluent. (c) SEC curves of CB3 using H_2O as an eluent. (d) Typical AFM height images of BB and CB in dilute water solutions. (e) TEM images of CB3 at pH 7.4. (f) Hydrodynamic diameters of CBs in water and PBS measured by DLS. (g) Zeta potential of CBs in different media. (h) TEM images of CB3 at pH 5.5 and (i) hydrodynamic diameters of CBs at pH 5.5.

well as the complete absence of the azide group (2000–2100 cm^{-1}) after cyclization can be observed in the FTIR spectra (Fig. S4, ESI†), which both support the successful cyclization.

In order to explore whether a dual-function lubricating and pH-responsive controlled release system has a good therapeutic effect on OA or not, we meticulously designed the water-soluble cyclic brush zwitterionic polymer CB. Compared with the ^{1}H NMR spectrum of *c*-P(HEMA-Br)$_{50}$ (Fig. S5, ESI†), the DP of DMAEMA and SBMA in CB were determined to be ~30 and ~45, respectively (Fig. S6, ESI†). As can be seen, the proton signals of the SBMA and DMAEMA are observed at 4.5, 3.75, 3.25, and 2.25 ppm and 4.1, 2.6, and 2.25 ppm in the CB spectrum, respectively. Likewise, the successful synthesis of the remaining three cyclic brush polymers and bottle-brush polymers was also demonstrated

by ^{1}H NMR and SEC (Fig. S7–S13, ESI†). As shown in Fig. 1c and Fig. S11–S13 (ESI†), CB1, CB2, CB3, CB4 and BB all display unimodal molecular weight distribution.

Atomic force microscopy (AFM) was employed to provide insight into the morphology of two types of polymer brushes. As shown in Fig. 1d and Fig. S14, S15 (ESI†), the wormlike morphology of BB and the cyclic brush morphology of CB convincingly support the successful polymer synthesis. The TEM results also show that the four types of CBs are regular spherical micelles and well-dispersed, supporting that all self-assembled micelles have excellent colloidal stability (Fig. 1e and Fig. S16a–c, ESI†). We further measured the hydrodynamic sizes of CB and BB by dynamic light scattering (DLS) as well as their zeta potentials in deionized water and physiological conditions (PBS, pH 7.4). The particle size is related to the self-assembly behavior of polymer micelles. In deionized water and buffer at pH 7.4, micelles can stably self-assemble, possessing a hydrodynamic diameter exceeding 70 nm with a slight difference (Fig. 1f), which confirmed that the CB cyclic brush topology enhanced colloid stability. In buffer at pH 5.5, the micelle undergoes disassembly, resulting in a smaller particle size (Fig. 1i). Nevertheless, their potentials show big differences. As shown in Fig. 1g, the zeta potential of CB in deionized water is significantly higher than that of in buffer solutions at pH 5.5 and 7.4, due to the strong binding of the trivalent phosphate negative ions with positively charged polymer micelles in phosphate buffer solution, shielding the positive charge properties of the micelle surface. In a buffer at pH 5.5, CB undergoes disassembly, more DMAEMA chains were exposed and protonation increased, resulting in a higher zeta potential compared to that at pH 7.4. TEM results visually showed that the micelle morphology changed, and the particle size decreased at pH 5.5 (Fig. 1h and Fig. S16d–f, ESI†). The BB polymers showed similar properties to the CB polymers (Fig. S17, ESI†). All the above results, including elemental analysis (EA) and scanning electron microscopy (SEM) (Fig. S18, ESI†), confirmed the successful synthesis of cyclic brush zwitterionic polymers.

Lubrication and wear properties

Lubrication plays a pivotal role in maintaining the daily activities of organisms, and reducing friction and wear is crucial for

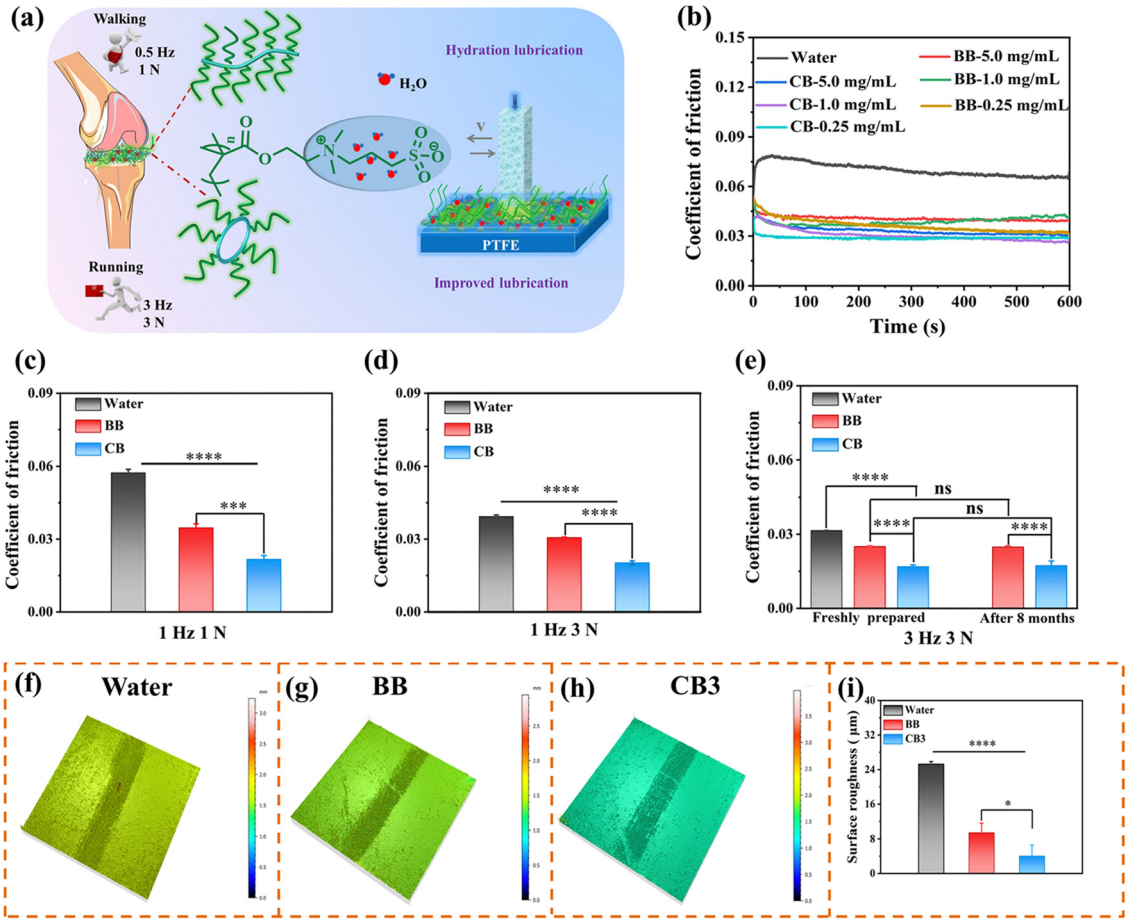

Fig. 2 The lubrication and wear properties of superlubricated CB. (a) Schematic diagram of the tribological test: frequency and stress of human joints in walking and running states. (b) COF-Time curve at 5.0 mg mL^{-1}, 1.0 mg mL^{-1} and 0.25 mg mL^{-1} of BB and CB. COF histograms for water, BB and CB (0.25 mg mL^{-1}) at (c) 1 Hz, 1 N; (d) 1 Hz, 3 N. (e) COF histograms of freshly prepared and stored for 8 months of BB and CB at 3 Hz, 3 N. Three-dimensional wear surface topographies: after friction tests with (f) water, (g) BB and (h) CB as lubricant. (i) Statistical histograms of surface roughness R_a of water, BB and CB (n = 3, *p < 0.05, ***p < 0.001, ****p < 0.0001).

relieving pain from OA. Although numerous studies have shown that zwitterions and brush-like topologies can effectively reduce friction and improve lubrication,[10–12] the lubricating properties of cyclic brush zwitterions have not been studied so far. Based on this, we conducted tribological experiments in reciprocating mode using UMT-3 to investigate the lubricating properties of CB and BB (Fig. 2a). As shown in Fig. 2b, compared with water with a coefficient of friction (COF) value of 0.08, the COF values of different concentrations of CB and BB significantly reduced to ~0.04 at 0.5 Hz, 1 N. The significantly improved lubricating performance is attributed to the zwitterionic charges ($-N^+(CH_3)_2-$ and $-SO_3^-$) of PSBMA brush side chains, which attracted a large number of water molecules through ionic coupling, forming a stable hydrated lubricating layer.[45,46] It should be noted that there is no significant difference between the COF values of 1 mg mL^{-1} and 0.25 mg mL^{-1}. Therefore, we selected the concentration of CB and BB at 0.25 mg mL^{-1} for subsequent cell and animal experiments. The effects of different frequencies and loads on the lubrication performance of CB and BB were further evaluated (simulating the frequencies and loads at the joints of human walking and running). The COF-histograms and time curves are shown in Fig. 2c–e and Fig. S19 (ESI†). It can be seen that with the increase of the reciprocating friction frequency and load, the COF values of CB and BB are significantly lower than those of the water group (1 Hz, 1 N: water: 0.057, BB: 0.035, CB: 0.022; 1 Hz, 3 N: water: 0.039, BB: 0.031, CB: 0.02; 3 Hz, 3 N: water: 0.032, BB: 0.025, CB: 0.017), which may be due to the mixed lubrication mechanism, *i.e.*, the combined effect of hydrodynamic lubrication and boundary lubrication.[47,48] It is worth noting that under the same conditions, the lubricating ability of CB is significantly better than that of BB (COF decreased by ~32%), which may be attributed to the inherent cyclic topology of CB. Compared with the bottle brush, the cyclic brushes are not staggered due to the absence of polymer chain ends, thus suppressing the interfacial interfingering with the bottlebrush-like anti-surface, thus possessing higher steric stability. It is noteworthy that the COF value of BB and CB barely changed after 8 months of storage and the COF of CB was very stable at 0.018 during the whole 10 000 cycles, implying that CB has super stable long-term lubricity (Fig. 2e and Fig. S20, ESI†). However, there was almost no difference in the COF values of the four cyclic brushes throughout the friction test, which was undoubtedly attributed to the same cyclic core and the same chain length of SBMA (Fig. S21, ESI†). These unique properties endow CB with super lubricated properties, which may spark great interest in designing long-acting lubricants for tribological applications.

To further analyse the friction properties of CB and BB, the wear surface morphology after tribological experiments was observed by confocal laser scanning microscopy (CLSM). Compared with unworn polytetrafluoroethylene (PTFE, blank), the three-dimensional wear surface morphology of deionized water, BB and CB lubricants is obvious. As shown in Fig. 2f–h and Fig. S22 (ESI†), we can intuitively see that the wear of water as a lubricant is the deepest, and the wear of CB is the shallowest. The surface roughness (R_a) of the unworn PTFE was only 1.347 mm, while the surface roughness of all PTFEs changed significantly after the friction test. In detail, the R_a value of CB is the smallest at 4.011 mm, followed by BB at 9.424 mm, and the value of water (25.273 mm) is the largest (Fig. 2i). Overall, these results suggested that compared to other groups, as a novel lubricant, CB can not only provide excellent lubrication ability, but also significantly reduce wear, which is instrumental in reducing cartilage wear in OA treatment.

In vitro drug loading, drug release and ROS scavenging

In order to avoid premature separation caused by excessive dilution of body fluids when drugs are applied to organisms, the delivery of two (or more) active pharmaceutical ingredients with spatiotemporal consistency is conducive to precision medicine and synergistic therapeutics, which has been widely used in the combined treatment of various diseases.[31] Here, the four types of CBs were loaded with Cur and LXP, respectively, and their drug loading (DLC) and encapsulation rate (EE) are shown in Tables S4 and S5 (ESI†). Interestingly, CB3 showed the highest DLC and EE in both Cur (DLC: 18.6%, EE: 92.9%) and LXP (DLC: 16.5%, EE: 82.7%), which may be attributed to its optimal hydrophilic and hydrophobic ratios. Therefore, CB3 (named CB) and the corresponding bottle brush polymer (BB) were selected as the model polymers to encapsulate Cur and LXP through hydrophobic and electrostatic interactions, and the pH-responsive CB and BB drug controlled release systems were successfully prepared (Fig. S23a, ESI†). The UV absorption spectra and standard curves of Cur and LXP are shown in Fig. S23b–e (ESI†). The DLC and EE of BB@Cur@LXP and CB@Cur@LXP were 21.7% and 77.8%, 27.4% and 84%, respectively. Encouragingly, both CB and BB reported here show higher drug loading efficiency compared to the previously reported drugs of polymer micelles with different morphologies by physical entrapment[14,43,49–56] and drugs of brush polymers by chemical binding[57,58] (Fig. 3a). CB@Cur@LXP has a greater drug loading capacity than BB@Cur@LXP, which may be due to the greater stability of CB@Cur@LXP, which can better encapsulate drug molecules.[44] Cumulative release studies of Cur and LXP drugs were evaluated under physiological (pH 7.4) and acidic (pH 5.5) conditions, respectively (Fig. 3b–e), simulating the mixed pH of the OA microenvironment. Apparently, all curves have two phases, the burst release phase and the relative plateau phase, which is similar to previous studies on physical entrapment of drugs. The cumulative release profiles of Cur and LXP at pH 7.4 over 14 days were similar, that is, the release was almost constant over time. Due to the pH-responsive cleavage of DMAEMA, an acid-responsive release behavior was observed for both Cur and LXP-loaded BB and CB at pH 5.5. Both drug profiles showed rapid drug release during the first 4 days, followed by a relative plateau. The rapid release of CB was attributed to the disassembly of the micelles under acidic conditions, which agrees well with the DLS-monitored micelle destabilization at the acidic pH of 5.5. Notably, the release rate of LXP was significantly faster than that of Cur, which may be explained by the rapid disintegration of brush-loaded LXP through electrostatic interaction, beneficial for the treatment of early OA. The slower release of Cur loaded in the hydrophobic

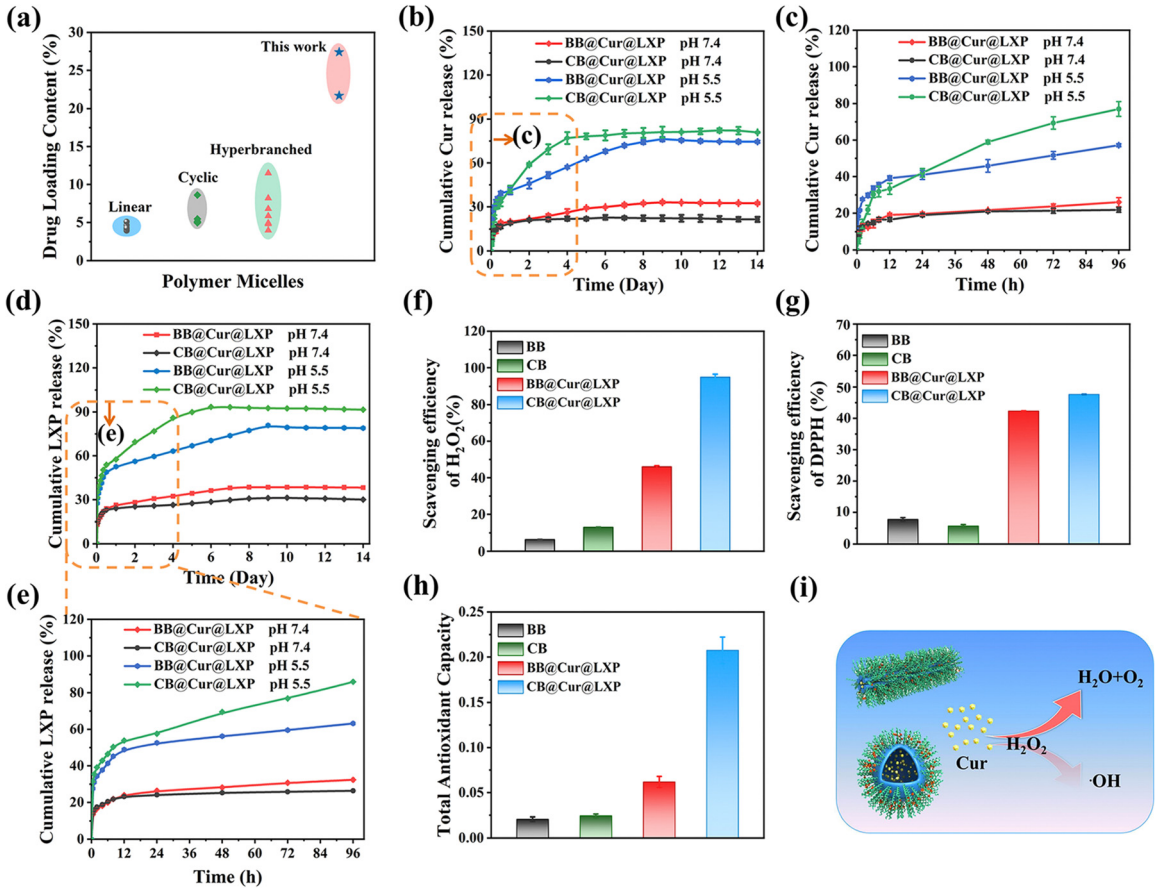

Fig. 3 *In vitro* drug loading, drug release and antioxidant activity. (a) Drug loading content of CB, BB, and the comparison with different morphologies reported. (b–e) Drug release profiles of the Cur (b: 14 day and c: the first 96 h) and LXP (d: 14 day and e: the first 96 h) from BB@Cur@LXP and CB@Cur@LXP. The scavenging efficiency of (f) H_2O_2 and (g) DPPH by BB, CB, BB@Cur@LXP and CB@Cur@LXP at 0.25 mg mL^{-1}, respectively. (h) Total antioxidant capacity of BB, CB, BB@Cur@LXP and CB@Cur@LXP and (i) schematic diagram of antioxidant mechanism.

core can further alleviate OA. The drug release rate is a key parameter to ensure high drug activity, and the combined effect of early rapid response release and plateau slow release is more conducive to improving drug efficacy.[59] We further fitted the drug release curves, as shown in Tables S6 and S7 (ESI†), and the release kinetics of BB@Cur@LXP and CB@Cur@LXP in different release media were consistent with the Korsmeyer–Peppas model because of the highest correlation coefficient ($R^2 \geq 0.94$). It is worth noting that polymer undergoes disassembly at pH 5.5, and more DMAEMA chains were exposed and have electrostatic and hydrogen bond interactions with loaded drugs, which affects drug release behavior as well as drug release fitting curve (Fig. S24 and S25 ESI†). In summary, CB not only has superlubricated properties, but also can be used as an effective carrier; on the one hand this can prevent the rapid loss of drugs, improve the bioavailability of drugs, and on the other hand, it can also achieve dual-drug controlled release. Therefore, the designed superlubricated dual drug CB@Cur@LXP could achieve pH-responsive specific controlled release behavior of preloaded drugs under local and intra-articular injection.

Excessive friction in joints can induce oxidative stress, induce chondrocytes to produce reactive oxygen species (ROS), and then lead to arthritis.[60,61] Based on the antioxidant activity of Cur, we first evaluated the H_2O_2 scavenging ability of all formulations with a hydrogen peroxide assay kit after studying the lubrication and controlled release properties of CB. As shown in Fig. 3f, the H_2O_2 scavenging efficiency of CB@Cur@LXP reached 95%. This excellent result was attributed to the higher Cur loading in the CB. DPPH is often used as a free radical to evaluate antioxidant activity.[62] As shown in Fig. 3g, the DPPH scavenging rate of each group was 7.7%, 5.7%, 42.3%, and 47.6%, respectively, and the CB still showed the best DPPH inhibition ability. Finally, the total antioxidant capacity of the materials was evaluated by the total antioxidant capacity assay kit (FRAP method), and CB@Cur@LXP reached 0.208 (Fig. 3h), which was consistent with the scavenging efficiency of H_2O_2 and DPPH. The ROS scavenging mechanism is shown in Fig. 3i. In summary, CB@Cur@LXP can significantly enhance the antioxidant activity, thereby effectively scavenging ROS.

In vitro cell viability, cytotoxicity and intracellular ROS scavenging

To evaluate the feasibility of CB@Cur@LXP for OA treatment, it is necessary to investigate the biocompatibility and protective effects of the material *in vitro*. We first evaluated the *in vitro* cell

viability and cytotoxicity of BB, CB, BB@Cur@LXP and CB@Cur@LXP on rat chondrocytes by CCK-8 assay and live/dead Kit staining. As shown in Fig. 4a and b, there was no significant difference between the experimental groups and the control group, and even at a concentration of 250 μg mL^{-1}, the survival rate of cells in each group remained above 80%. Intriguingly, CB@Cur@LXP showed better cell survival rate than the other groups at different concentrations, indicating that CB@Cur@LXP had negligible effects on chondrocyte viability and proliferation. The results of live/dead staining showed that chondrocytes had metabolic activity, and almost all the live cells (stained green) were in the microscopic fields at different time points, while the dead cells (stained red) were few, and the cell density increased sharply from day 3 to day 5 (Fig. 4c). From day 1 to day 5, the number of live cells increased with the increase of culture time, and there was still no significant difference between the experimental groups and the control group at different time points (Fig. 4d). In addition, morphological staining experiments showed that all cells were morphologically healthy, with prominent pseudopodia and were spindle-shaped (Fig. 4e). The *in vitro* cell results collectively confirmed the good biocompatibility of the CB@Cur@LXP and its nontoxicity to chondrocytes, which is a prerequisite for *in vivo* experiments.

The anti-inflammatory drug Cur has a certain antioxidant pharmacological activity, 2,7-dichlorodihydrofluorescein diacetate (DCFH-DA) was used as a fluorescent probe to study the intracellular ROS scavenging ability of BB, CB, BB@Cur@LXP and CB@Cur@LXP. The expression levels of ROS in the BB and CB were not significantly different from those in the control group, while the BB@Cur@LXP and CB@Cur@LXP significantly inhibited the expression of intracellular ROS, and the ROS inhibition was more significant in the CB@Cur@LXP, which was attributed to the higher Cur drug loading (Fig. S26, ESI†). This was consistent with the above-mentioned extracellular ROS scavenging effect.

In vitro anti-inflammatory effect

Chondrocytes are the only cellular component of articular cartilage and have dual functions of regulating cartilage synthesis and catabolism. The pathogenesis of OA is affected by a

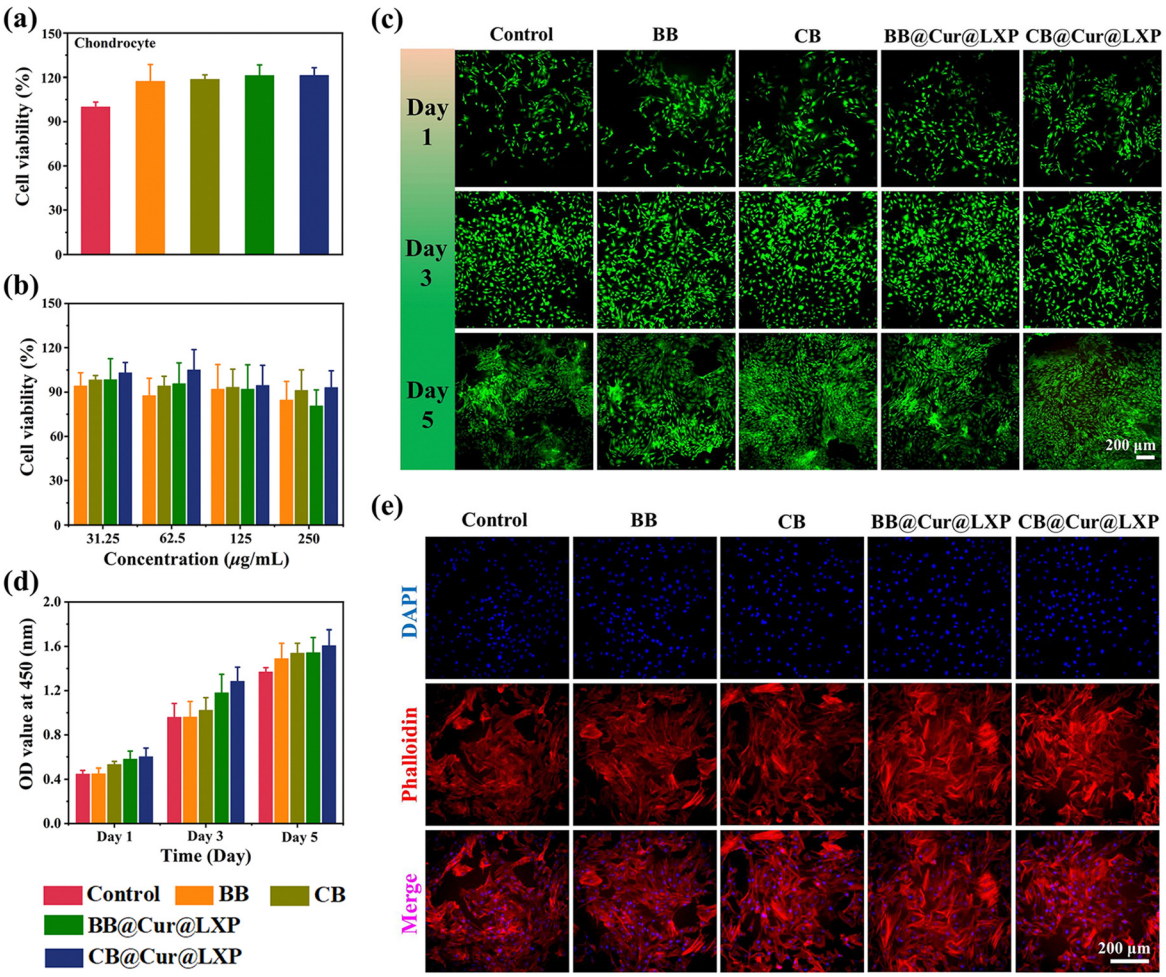

Fig. 4 *In vitro* biocompatibility of CB@Cur@LXP. (a and b) CCK-8 assay demonstrates the cell viability of chondrocytes co-cultured with the BB, CB and BB@Cur@LXP and CB@Cur@LXP at day 1. (c) Representative fluorescence images displaying live/dead staining assay of chondrocytes and (d) chondrocytes proliferation with different groups co-cultured for 1, 3 and 5 days. (e) Cell morphology of chondrocytes with different groups after culturing for 1 day, red: FITC-Phalloidin (cytoskeleton); blue: DAPI (nucleus).

variety of factors, including pro-inflammatory cytokines (IL-1β, IL-6), synthetic genes (Aggrecan, Col2α), and catabolism genes (MMP13 and TAC1, *etc.*).[63] These factors interfere with cartilage synthesis and catabolism by inhibiting the expression of proinflammatory cytokines, as well as regulating the synthesis and degradation related enzymes of the cartilage matrix. To examine the protective effect of CB@Cur@LXP on chondrocyte degradation *in vitro*, in this study, lipopolysaccharide (LPS) activated inflammation models are used to simulate the inflammatory microenvironment during the pathogenesis of OA. The LPS-induced chondrocytes were co-cultured with BB, CB, BB@Cur@LXP and CB@Cur@LXP for 24 h and the expression levels of each gene by qRT-PCR were analysed to evaluate the anti-inflammatory effect of CB@Cur@LXP (Fig. 5a). As expected, LPS treatment significantly down-regulated Aggrecan and Col2α1 expression, while IL-1β, MMP13, TAC1 and Adamts5 expression were up-regulated. Subsequently, we further investigated the mRNA expression after the addition of BB, CB, BB@Cur@LXP and CB@Cur@LXP, respectively. Compared with the control group, the BB@Cur@LXP and CB@Cur@LXP significantly reversed mRNA relative gene expression, but the effect was limited in the BB and CB. As shown in Fig. 5b and c, BB@Cur@LXP and CB@Cur@LXP could promote the expression of anabolic factors, such as Aggrecan and Col2α1, thereby protecting chondrocytes to a certain extent. On the other hand, the mRNA expressions of IL-1β (Fig. 5d), MMP13 (Fig. 5e), TAC1 (Fig. 5f) and Adamts5 (Fig. 5g) in the BB@Cur@LXP and CB@Cur@LXP were significantly decreased, which was similar to that in the control group (normal chondrocytes). Notably, the expression levels of the six genes were more significantly changed in the CB@Cur@LXP treatment group, which was attributed to the increased lubrication (topological effect and zwitterion hydration lubrication) and dual-drug anti-inflammatory effect. In addition, the slight changes in mRNA gene expression in BB and CB treated groups suggested that lubrication could also reduce inflammation and pain. In short, CB@Cur@LXP has good cartilage protection potential for inflammation-induced chondrocyte degeneration, which can effectively inhibit inflammation and reduce pain. Therefore, the CB@Cur@LXP designed in this study is the ideal biomaterial to protect chondrocytes from inflammatory invasion.

In vivo therapeutic effect of osteoarthritis

The above results proved that CB@Cur@LXP possessed properties required for the treatment of early OA. Furthermore, to assess the *in vivo* therapeutic effect of CB@Cur@LXP on OA, the OA model on SD rat was established by transection of the medial meniscus (DMM), as shown in Fig. 6a. One week after surgery, normal saline (NS), BB, CB, BB@Cur@LXP and

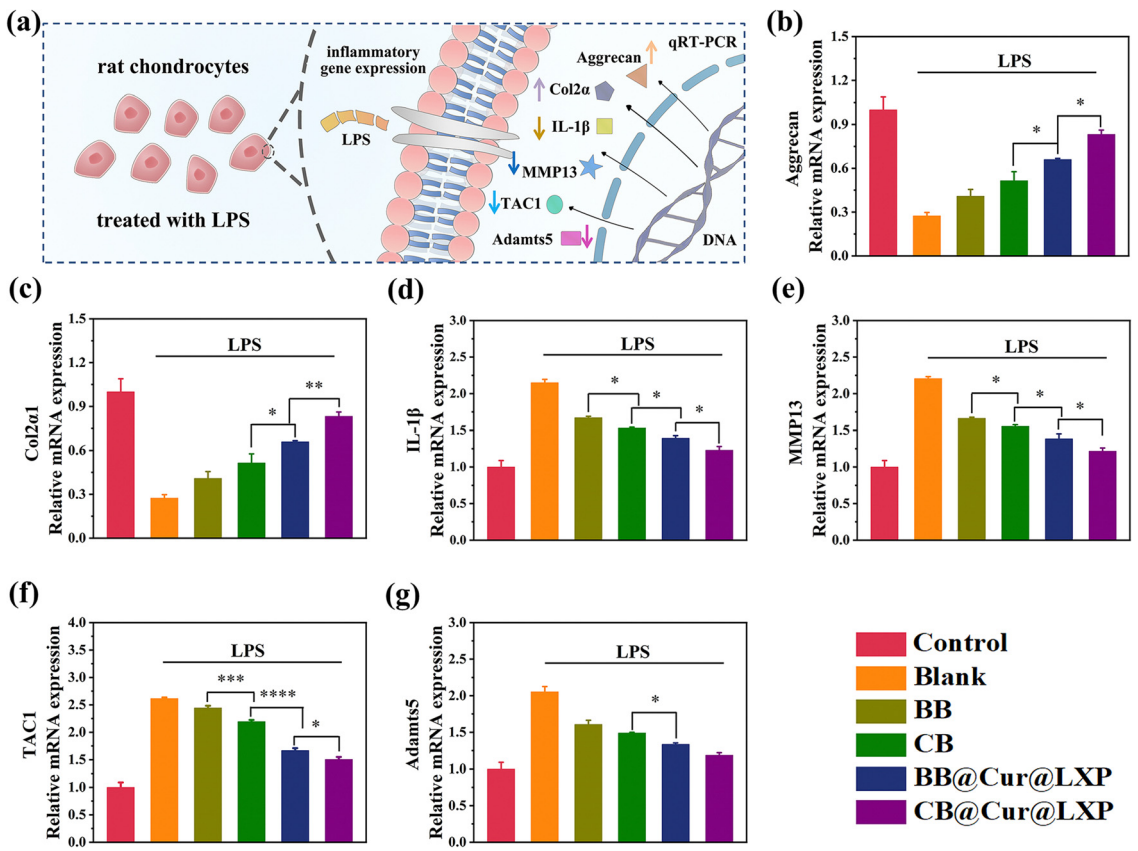

Fig. 5 *In vitro* protective effect of CB@Cur@LXP on chondrocytes. (a) Experimental design to simulate inflammatory microenvironment of OA. qRT-PCR analysis shows the mRNA expression levels of (b) Aggrecan, (c) Col2α1, (d) IL-1β, (e) MMP13, (f) TAC1 and (g) Adamts5 in the LPS-treated chondrocytes, which are co-cultured with the BB, CB, BB@Cur@LXP and CB@Cur@LXP for 24 h (n = 3, *p < 0.05, **p < 0.01, ***p < 0.001 and ****p < 0.0001).

CB@Cur@LXP were injected into the articular cavity once every 2 weeks for 8 consecutive weeks in randomized rats, the control group is the healthy SD rat injected by NS for comparison. All rats survived well after surgery without signs of infection. After 8 weeks of treatment, rats in all groups were euthanized, and the knee joints were carefully separated. As shown in Fig. 6b, the femoral condyle and tibia in the OA group have obvious erosion and osteophyte formation, indicating successful knee OA. Compared with the control group with the lowest total osteophyte volume, the osteophyte volume of the five treatment groups was significantly increased, *i.e.*, OA group (3.98 mm^3), BB (3.17 mm^3), CB (2.69 mm^3), BB@Cur@LXP (2.41 mm^3) and CB@Cur@LXP (1.81 mm^3) (Fig. 6c). Compared with the OA group, the osteophyte volume of the CB@Cur@LXP significantly decreased by 54.5%, followed by BB@Cur@LXP and CB 39.4% and 32.4% reduction, respectively, and no significant reduction in BB (~20.4%). The CB@Cur@LXP was significantly better than the other groups, indicating that CB played an important role in inhibiting the development of osteoarthritis. The CB@Cur@LXP achieved optimal results through the synergistic effect of enhanced lubrication (inhibiting early OA) and specific administration (interfering with late OA). In conclusion, Micro-CT demonstrated that after treatment with CB@Cur@LXP, the cartilage surface was the smoothest and the osteophyte volume was the smallest, which was closest to the control group, indicating that CB@Cur@LXP could alleviate joint injury and thus inhibit osteophyte formation.

To further evaluate the *in vivo* anti-inflammatory effect of CB@Cur@LXP, the expression of specific inflammatory factors, such as aggrecan (Fig. 6d), Col2α1 (Fig. 6e), MMP13 (Fig. 6f), Adamts5 (Fig. 6g) and TAC1 (Fig. 6h) in cartilage samples were detected by qRT-PCR. Compared with the control group, the OA group significantly downregulated the expression of aggrecan and Col2α1 anabolic genes, and upregulated the expression of MMP13, Adamts5 catabolic gene and pain-related gene TAC1, indicating severe joint inflammation. After treatment with different groups, anabolic genes, catabolic genes and pain genes were reversed to varying degrees, among which BB and CB partially increased the expressions of aggrecan and Col2α1, and had limited inhibitory effects on MMP13, Adamts5 and TAC1. Compared with the CB, BB@Cur@LXP and CB@Cur@LXP had more obvious regulation effects on various genes, significantly inhibited the expressions of MMP13, Adamts5 and TAC1, and up-regulated the expressions of aggrecan and Col2α1. The inflammatory regulation effect of CB@Cur@LXP was more effective, almost the same as the gene expression of

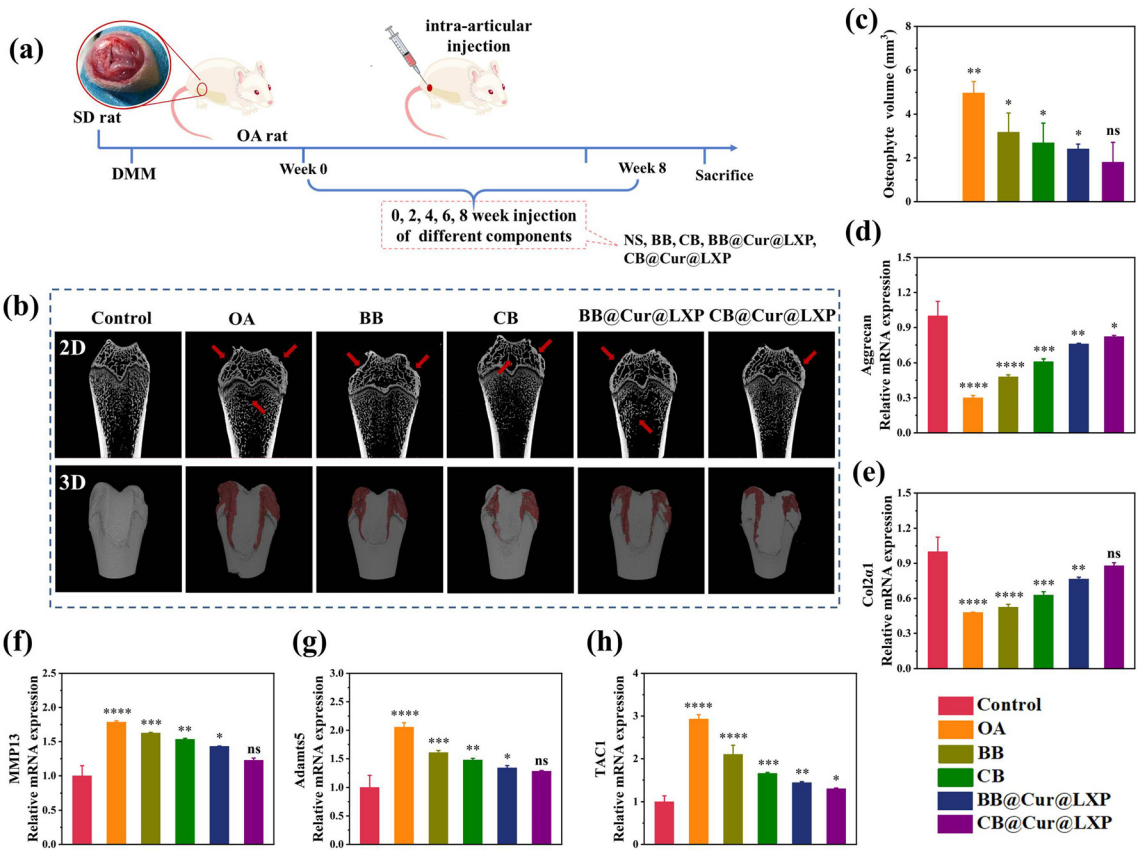

Fig. 6 Therapeutic effect of CB@Cur@LXP on DMM-induced OA rats. (a) Schematic illustration of treatment regimens. (b) Representative Micro-CT images of knee joint at 8 weeks after DMM surgery. Red arrows of 2D and red shading of 3D indicate the osteophytes. (c) The total osteophyte volume at 8 weeks after DMM surgery. qRT-PCR analysis shows the expression levels of inflammatory cytokines (d) Aggrecan, (e) Col2α1, (f) MMP13, (g) Adamts5 and (h) TACI *in vivo* after BB, CB, BB@Cur@LXP and CB@Cur@LXP treatment (n = 3, *p < 0.05, **p < 0.01, ***p < 0.001 and ****p < 0.001 when compared with control).

the control group. Therefore, the results confirmed that CB@Cur@LXP, acting as a superlubricated anti-inflammatory agent, significantly promotes the production of anabolic genes, inhibits the production of catabolic genes, relieves pain, and has a significant anti-inflammatory effect on OA.

Micro-CT showed significant osteophyte reduction, and qRT-PCR also confirmed the excellent anti-inflammatory properties of the CB@Cur@LXP. However, it did not provide specific information on the interaction between the superlubricated controlled-release material and the process of cartilage regeneration. To further determine whether the designed biomaterials could delay the progression of OA, decalcified tissue specimens were sectioned 8 weeks after surgery, and histological hematoxylin and eosin (H&E) staining, safranin O/fast green staining, Masson's trichrome staining and collagen II staining were performed. The H&E staining (Fig. 7a) shows that the chondrocytes of control group were neatly and tightly arranged, and the articular cartilage surface was smooth and continuous, while typical morphological features of OA were observed in the saline group, such as the discontinuous surface, erosion, cracks and obvious chondrocyte degeneration or necrosis. The CB, BB@Cur@LXP and CB@Cur@LXP all showed varying degrees of improvement in morphological change and matrix staining compared with OA and BB. Notably, compared with the OA group, the degree of cartilage lesions in CB@Cur@LXP was the most significantly improved, in which abundant bone marrow cells in the bone marrow cavity, complete and normal articular cartilage matrix morphology, normal overall staining, and less chondrocyte degeneration or necrosis can be clearly observed, indicating that OA progression has been inhibited to the greatest extent, confirming that functionalized CB@Cur@LXP could effectively delay the *in vivo* progression of osteoarthritis. The staining of safranin O-fast green can also indirectly reflect the content and distribution of glycosaminoglycan in the cartilage matrix. The staining of the cartilage of the control group was clear and uniform, while that of the OA group was shallow and uneven (Fig. S27, ESI†). The CB@Cur@LXP cartilage glycosaminoglycan (red staining) level was the highest, indicating that combined treatment with two drugs could preserve the attenuation of cartilage matrix more effectively on the basis of lubrication. Furthermore, Masson's trichrome staining showed that the collagen staining of the CB@Cur@LXP was significantly higher than that of the BB@Cur@LXP, CB and BB (Fig. 7b). To evaluate the collagen fibers of new bone in detail, three different areas of the same sample were selected under a 40× microscope to calculate the collagen area. As shown in Fig. 7c,

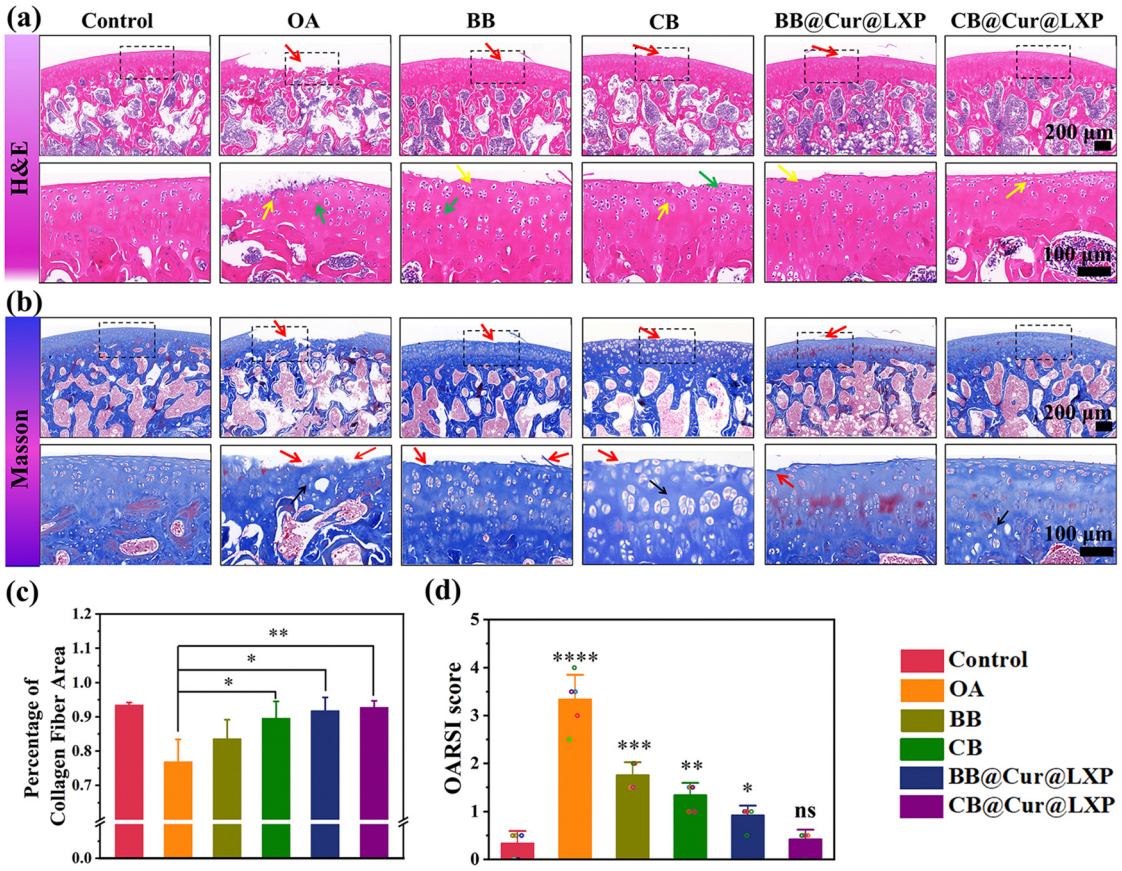

Fig. 7 CB@Cur@LXP can delay the progression in rats of osteoarthritis. Representative images of (a) H & E staining and (b) Masson's trichrome staining. Red arrow represents erosion defect of articular cartilage, yellow arrow indicates degeneration or necrosis of chondrocytes, and green arrow shows disappearance of chondrocyte bone lacunae. (c) The proportion of articular cartilage collagen fiber area in each group, (d) OARSI score of articular cartilage in each group (n = 5, *p < 0.05, **p < 0.01, ***p < 0.001 and ****p < 0.001).

compared with the OA group, the collagen area of each group increased to varying degrees, among which the collagen area of CB@Cur@LXP was closest to that of the control group, confirming that CB@Cur@LXP promoted the maturation of new collagen fibers around the cartilage. All groups were scored based on the degree of cartilage damage according to osteoarthritis research society international (OARSI) (Fig. 7d),[64] compared with the control group, the OARSI scores of other treatment groups were different, among which the CB@Cur@LXP had no significant difference (ns), followed by BB@Cur@LXP ($p < 0.05$), the CB ($p < 0.01$), and BB ($p < 0.001$). The above results indicate that the progression of OA in the CB@Cur@LXP has been inhibited to the greatest extent, including the improvement of the degree of cartilage lesions, the recovery of cartilage morphology, the deposition of glycosaminoglycans, the increase of collagen fiber area and the decreased OARSI score.

Collagen staining was further carried out to evaluate the regeneration of collagen. Fig. S28 (ESI†) showed even and obvious Col2α expression in the control group, while there were fewer positive staining cells in the OA group (brown). After treatment, the positive cells in BB@Cur@LXP and CB@Cur@LXP are significantly increased, and the expression of collagen II was the most obvious in CB@Cur@LXP, which was attributed to the synergistic lubrication and anti-inflammatory properties. Overall, CB@Cur@LXP, designed for the first time in this work has the synergistic properties of super lubricity, controlled drug release and anti-inflammatory effects, which can effectively reduce osteophyte formation and inhibit cartilage degeneration, thus providing the most attractive strategy for the OA treatment.

The biosafety of materials is another important criterion for biomedical applications. Therefore, we evaluated the long-term systemic toxicity of each treatment group by hematology and histological analysis.[65] First, the levels of inflammatory cytokines interleukin-6 (1L-6), tumor necrosis factor (TNF-α) and prostaglandin E2 (PGE2) in serum samples from SD rats were assessed by enzyme-linked immunosorbent assay (ELISA). As shown in Fig. S29 (ESI†), there was no significant difference between the groups, indicating that local administration did not cause systemic toxicity, confirming the good biosafety of all groups. Furthermore, the blood parameters of SD rats were similar to those of the control group and were all within the normal range, indicating the desirable blood safety of CB@Cur@LXP (Fig. S30, ESI†). In addition, the H & E staining of the major organs (heart, liver, spleen, lungs, and kidneys) of SD rats in all groups had no obvious tissue damage or pathological changes (Fig. S31, ESI†). Therefore, the long-term biosafety evaluation confirmed that CB@Cur@LXP has good biocompatibility and biosafety *in vivo*, further confirming its potential for clinical application in OA.

Conclusions

In conclusion, we designed and synthesized for the first time a novel superlubricated, pH-responsive anti-inflammatory dual drug delivery platform based on cyclic brush zwitterionic polymers (*c*b-P(HEMA-*g*-P(DMAEMA-*st*-SBMA)), CB) for OA treatment. Four functional cyclic brush polymers CB1, CB2, CB3 and CB4 were prepared *via* a click-reaction, ATRP reaction and self-assembly. The tribological experiment showed significantly enhanced lubrication of CB (COF ∼ 0.017) than BB, which was owing to the hydration lubrication of the zwitterionic groups in SBMA and the topological effect of the cyclic brush. In particular, the special structure of the cyclic brush polymer can simultaneously encapsulate the anti-inflammatory hydrophobic drug Cur and hydrophilic drug LXP to achieve a high drug loading, then realize the rapid release of LXP and the slow and long-acting release of Cur according to the pH-responsive behavior, so as to achieve long-term OA treatment. In addition, *in vitro* and *in vivo* experiments demonstrated that the superlubricated CB@Cur@LXP with good biocompatibility could not only protect chondrocytes from inflammatory factor-induced degeneration *in vitro*, but also effectively inhibit the development of OA in the rat DMM model, that is, reduce osteophytes and cartilage degradation. More importantly, the CB@Cur@LXP up-regulated articular cartilage anabolic genes and down-regulated catabolic proteases. Overall, the superlubricated cyclic brush zwitterionic polymers (*c*b-P(HEMA-*g*-P(DMAEMA-*st*-SBMA)), CB) synthesized in this study not only provide valuable insights for the design of dual-drug local drug delivery systems, but the injectable CB@Cur@LXP can be a potential for the treatment of OA and other clinical diseases. Currently, the research work has obtained Invention Patent Grant (Chinese patent no. ZL 2022 1 0489057.7, authorization notice no. CN 114933677 B). In the future, we will continue to carry out clinical research of this work.

Experimental

Synthesis of pH-sensitive bottle brush and cyclic brush copolymers, bb-P(HEMA-*g*-P(DMAEMA-*st*-SBMA)) (BB) and cb-P(HEMA-*g*-P(DMAEMA-*st*-SBMA)) (CB)

Novel pH-sensitive bottle brush and cyclic brush copolymers were synthesized by "one-pot" ATRP of [2-(methacryloyloxy)ethyl]dimethyl-(3-sulfopropyl)/2-(dimethylamino) ethyl methacrylate (SBMA/DMAEMA) using *l*-P(HEMA-Br)$_{50}$ and *c*-P(HEMA-Br)$_{50}$ as the multimacroinitiators, respectively. Taking the preparation of *c*b-P(HEMA-*g*-P(DMAEMA-*st*-SBMA)) as an example, c-P(HEMA-Br)$_{50}$ (3.5 mg), SBMA (207.75 mg), DMAEMA (157.21 mg), and bipyridine (bpy, 3.872 mg) were added into 2,2,2-trifluoroethyl alcohol (TFEA, 3.334 mL). After three freeze–pump–thaw cycles, CuBr (1.77 mg) was added under the protection of a nitrogen flow. After another three freeze–pump–thaw cycles, the reaction mixture was sealed and kept in an oil bath preheated at 60 °C. After the reaction completed, the solution was quenched by exposing to the air. The mixture was poured into ice-cold anhydrous diethyl ether to get the crude product. The crude product was purified by dialysis against distilled water to remove copper catalyst and any un-reacted monomer. The bottle brush (BB) and cyclic brush (CB) product were harvested by freeze-drying.

Lubrication properties

The lubrication properties of BB and CB lubricants were evaluated through tribological tests. Tribological tests were performed in reciprocating mode at room temperature on a multifunctional friction and wear tester (UMT-3, Bruker, USA). All the tribology experiments adopted the ball-disk friction test mode, and Si_3N_4 ball and polytetrafluorethylene (PTFE) was used as upper and lower friction pairs. The sliding amplitude was set to 3 mm. Friction tests were performed for 10 min at different lubricant concentrations (0.25–5.0 mg mL^{-1}), loads (1–3 N) and frequencies (0.5–3 Hz). The curves of the friction coefficient (COF) of each lubricant with time were recorded under different concentrations, loads and frequencies to evaluate the lubrication performance of each lubricant. After the friction test, the surface roughness of the samples was observed using a confocal laser scanning microscope (Zeiss LSM799 MAT) to evaluate the wear performance.

Extracellular ROS scavenging activity

The ROS scavenging activity of CB@Cur@LXP was determined by DPPH, H_2O_2 and total antioxidant capacity, respectively. More details of the experiment are provided in the ESI.†

Study on *in vitro* drug loading, drug release and cytocompatibility of pH-sensitive bottle brush and cyclic brush polymers

We prepared dual drug BB@Cur@LXP and CB@Cur@LXP by loading a hydrophobic drug Cur and a negatively charged hydrophilic drug LXP respectively through hydrophobic and electrostatic interactions, and further studied the drug loading (DLC), encapsulation rate (EE) and *in vitro* drug release characteristics of various formulations. Then, *in vitro* cell viability, live/dead staining, morphological staining, and expression of inflammatory factors of chondrocytes co-cultured with BB@Cur@LXP and CB@Cur@LXP were investigated in detail.

In vivo study

All the experimental animal studies have the approval for animal ethics and welfare authorized by the Animal Ethics Committee of Sichuan University (KS2020028), from the Chengdu West China Experimental Animal Center (Chengdu, China). All animals were randomly divided into six groups to establish an SD rat model of osteoarthritis (8 weeks of age, 200–250 g, $n = 25$) by DMM surgery (Fig. 6a). One week after surgery, the rats in each group ($n = 5$ for each group) were injected with normal saline (NS), BB, CB, BB@Cur@LXP, CB@Cur@LXP, once every 2 weeks, and euthanized 8 weeks later. The anti-inflammatory and cartilage repair effects of the dual drug superlubricant were further evaluated by qRT-PCR, Micro CT and immunostaining. Finally, the biosafety of the material was evaluated by blood parameters and H & E staining of major organs. See the ESI† for specific experimental methods.

Author contributions

Miao Zhang: literature survey; polymer synthesis & characterization; data analysis; writing – original draft & revision. Xu Peng: DMM modeling and *in vivo* study in SD rats. Yuan Ding, Xiang Ke and Qiangwei Xin: cell and animal experiments help. Kai Ren: the friction test and data analysis. Meng Qin: performed data curation. Jing Xie: supervision; data analysis; writing – review, editing & revision; funding acquisition; Jianshu Li: supervision; conceptualization; data analysis; writing – original draft, review, editing & revision; funding acquisition.

Conflicts of interest

The authors declare that they have no known competing financial interests or personal relationships that could have appeared to influence the work reported in this paper.

Acknowledgements

This work was supported by the National Natural Science Foundation of China (no. 52073191, 51925304 and 52103176), and Sichuan Science and Technology Program (no. 2022NSFSC1949). The authors are grateful to Hong Xu (West China Hospital of Stomatology, Sichuan University) for his guideline for qRT-PCR data analysis.

Notes and references

1 W. J. Qiu, W. W. Zhao, L. D. Zhang, H. M. Wang, N. Y. Li, K. X. Chen, H. Y. Zhang and Y. G. Wang, *Adv. Funct. Mater.*, 2022, 2208189.
2 C. Corciulo, M. Lendhey, T. Wilder, H. Schoen, A. S. Cornelissen, G. Chang, O. D. Kennedy and B. N. Cronstein, *Nat. Commun.*, 2017, **8**, 15019.
3 Y. Han, J. Yang, W. Zhao, H. Wang, Y. Sun, Y. Chen, J. Luo, L. Deng, X. Xu and W. Cui, *Bioact. Mater.*, 2021, **6**, 3596–3607.
4 W. Zhao, H. Wang, H. Wang, Y. Han, Z. Zheng, X. Liu, B. Feng and H. Zhang, *Nanoscale*, 2021, **13**, 6394–6399.
5 T. Yong, X. Zhang, N. Bie, H. Zhang, X. Zhang, F. Li, A. Hakeem, J. Hu, L. Gan and H. A. Santos, *Nat. Commun.*, 2019, **10**, 3838.
6 W. D. Hou, C. Y. Ye, M. Chen, W. Gao, X. Xie, J. R. Wu, K. Zhang, W. Zhang, Y. Y. Zheng and X. J. Cai, *Bioact. Mater.*, 2021, **6**, 2439–2451.
7 T. Yamamoto and Y. Tezuka, *Soft Matter*, 2015, **11**, 7458–7468.
8 G. Morgese, L. Trachsel, M. Romio, M. Divandari, S. N. Ramakrishna and E. M. Benetti, *Angew. Chem., Int. Ed.*, 2016, **55**, 1–7.
9 G. Morgese, E. Cavalli, J.-G. Rosenboom, M. Zenobi-Wong and E. M. Benetti, *Angew. Chem., Int. Ed.*, 2018, **57**, 1621–1626.
10 X. Banquy, J. Burdyńska, D. W. Lee, K. Matyjaszewski and J. Israelachvili, *J. Am. Chem. Soc.*, 2014, **136**, 6199–6202.
11 G. Morgese, E. Cavalli, M. Müller, M. Zenobi-Wong and E. M. Benetti, *ACS Nano*, 2017, **11**, 2794–2804.
12 G. Morgese, S. N. Ramakrishna, R. Simic, M. Zenobi-Wong and E. M. Benetti, *Biomacromolecules*, 2018, **19**, 680–690.
13 M. Kapnistos, M. Lang, D. Vlassopoulos, W. Pyckhout-Hintzen, D. Richter, D. Cho, T. Chang and M. Rubinstein, *Nat. Mater.*, 2008, **7**, 997–1002.

14 Z. Liu, Y. P. Huang, X. L. Zhang, X. Y. Tu, M. Q. Wang, L. W. Ma, B. Y. Wang, J. L. He, P. H. Ni and H. Wei, *Macromolecules*, 2018, **51**, 7672–7679.
15 S. T. Milner, *Science*, 1991, **251**, 905–914.
16 J. Klein, *Science*, 2009, **323**, 47–48.
17 H. Chen, T. Sun, Y. F. Yan, X. L. Jia, Y. L. Sun, X. Zhao, J. Qi, W. G. Cui, L. F. Deng and H. Y. Zhang, *Biomaterials*, 2020, **242**, 119931.
18 L. Yang, L. Y. Sun, H. Zhang, F. K. Bian and Y. J. Zhao, *ACS Nano*, 2021, **15**, 20600–20606.
19 L. J. Kang, J. Yoon, J. G. Rho, H. S. Han, S. Lee, Y. S. Oh, H. Kim, E. Kim, S. J. Kim, Y. T. Lim, J. H. Park, W. K. Song, S. Yang and W. Kim, *Biomaterials*, 2021, **275**, 120967.
20 J. W. Orchard, *BMJ*, 2020, **368**, l6923.
21 D. T. Felson, *JAMA*, 2016, **316**, 2607–2608.
22 J. N. Katz, *JAMA*, 2021, **326**, 2012–2014.
23 B. Kristjansson and S. Honsawek, *Stem Cells Int.*, 2014, **2014**, 194318.
24 Y. F. Yan, T. Sun, H. B. Zhang, X. L. Ji, Y. L. Sun, X. Zhao, L. F. Deng, J. Qi, W. G. Cui, H. A. Santos and H. Y. Zhang, *Adv. Funct. Mater.*, 2019, **29**, 1807559.
25 Z. Q. Zhou, F. Gong, P. Zhang, X. T. Wang, R. Zhang, W. Xia, X. Gao, X. Z. Zhou and L. Cheng, *Nano Res.*, 2022, **15**, 3338–3345.
26 C. S. Kang, E. Jung, H. J. Hyeon, S. Seon and D. W. Lee, *J. Nanomed. Nanotechnol.*, 2020, **23**, 102104.
27 J. E. Hyun, D. W. Li, E. B. Lee and C. S. Jeong, *Arch. Pharm. Res.*, 2001, **24**, 541–545.
28 C. F. Liu, C. P. Li, C. Pang, M. Q. Li, H. X. Li, P. X. Li, L. Fan, H. Liu and W. Tian, *ACS Appl. Mater. Interfaces*, 2020, **12**, 27940–27950.
29 Y. Hu, C. H. Chen, Y. Y. Ding, X. Wen, B. Wang, L. Gao and K. Tan, *Nat. Commun.*, 2019, **10**, 2180.
30 X. D. Zhao, Y. X. Yang, J. Yu, R. Ding, D. D. Pei, Y. F. Zhang, G. He, Y. L. Cheng and A. Li, *Biomaterials*, 2022, **282**, 121387.
31 S. H. Li, R. Ma, X.-Y. Hu, H.-B. Li, W.-C. Geng, X. L. Kong, C. Zhang and D. S. Guo, *Adv. Mater.*, 2022, **34**, 2203765.
32 J. Salazar, L. Bello, M. Chávez, R. Añez, J. Rojas and V. Bermúdez, *Arthritis*, 2014, **2014**, 1–13.
33 F. A. Formica and G. Barreto, *J. Controlled Release*, 2019, **295**, 118–129.
34 T. Gui, L. J. Luo, B. Chhay, L. L. Zhong, Y. L. Wei, L. T. Yao, W. Yu, J. Li, C. L. Nelson, A. Tsourkas, L. Qin and Z. L. Chen, *Biomaterials*, 2022, **283**, 121437.
35 C. H. Evans, *Osteoarthritis Cartilage*, 2016, **24**, 1–3.
36 H. M. Hu, H. Ruan, S. Y. Ruan, L. X. Pei, Q. Jing, T. Wu, X. L. Hou, H. Xu, Y. J. Wang, N. P. Feng and Y. T. Zhang, *Chem. Eng. J.*, 2022, **431**, 134196.
37 H. M. Chen, Z. N. Qin, J. M. Zhao, Y. He, E. Ren, Y. Zhu, G. Liu, C. B. Mao and L. Zheng, *Biomaterials*, 2019, **225**, 119520.
38 F. Lin, Z. Wang, L. Xiang, L. F. Deng and W. G. Cui, *Adv. Funct. Mater.*, 2021, **31**, 2107678.
39 A. G. Bajpayee, C. R. Wong, M. G. Bawendi, E. H. Frank and A. J. Grodzinsky, *Biomaterials*, 2014, **35**, 538–549.
40 X. L. Xu, Y. Xue, J. Y. Ding, Z. H. Zhu, X. C. Wu, Y. J. Song, Y. L. Cao, L. G. Tang, D. F. Ding and J. G. Xu, *Acta Biomater.*, 2022, **154**, 23–48.
41 T. Yildirim, A. Traeger and P. Sungur, *Biomacromolecules*, 2017, **18**, 3280–3290.
42 A. Car, P. Baumann, J. T. Duskey, M. Cham, N. Bruns and W. Meier, *Biomacromolecules*, 2014, **15**, 3235–3245.
43 M. Zhang, Y. Liu, J. L. Peng, F. J. Liu, W. Ma, L. W. Ma, C.-Y. Yu and H. Wei, *Polym. Chem.*, 2020, **11**, 6139–6148.
44 M. Zhang, S. Li, J. L. Peng, Y. Liu, F. J. Liu, F. M. Zhong, S. S. Tang, Q. Ning, C.-Y. Yu and H. Wei, *Mater. Today Chem.*, 2022, **26**, 100996.
45 G. Q. Liu, Y. Feng, N. Zhao, Z. Chen, J. Q. Shi and F. Zhou, *Chem. Eng. J.*, 2022, **429**, 132324.
46 W. W. Zhao, Y. K. Yu, Z. Y. Zhang, D. M. He and H. Y. Zhang, *ACS Appl. Mater. Interfaces*, 2022, **14**, 35409–35422.
47 J. Klein, *Friction*, 2013, **1**, 1–23.
48 S. H. Loringa, R. E. Browna, A. Gouldstonea and J. P. Butler, *J. Biomech.*, 2005, **38**, 2390–2396.
49 W. Ma, G. Y. Kang, L. Sun, C. Meng, Y. Liu, Z. Zheng, M. C. Jiang, D. Wang, S. H. Pun, C.-Y. Yu and H. Wei, *J. Controlled Release*, 2022, **345**, 278–291.
50 G. Y. Kang, Y. P. Liu, L. X. Li, L. Sun, W. Ma, C. Meng, L. W. Ma, G. H. Zheng, C. Chang and H. Wei, *Chem. Commun.*, 2020, **56**, 3003–3006.
51 G. Y. Kang, L. Sun, Y. P. Liu, C. Meng, W. Ma, B. Y. Wang, L. W. Ma, C.-Y. Yu and H. Wei, *Langmuir*, 2019, **38**, 12509–12517.
52 Y. F. Wang, Z. Z. Wu, Z. W. Ma, X. Y. Tu, S. J. Zhao, B. Y. Wang, L. W. Ma and H. Wei, *Polym. Chem.*, 2018, **9**, 2569–2573.
53 Y. P. Liu, G. Y. Kang, L. Sun, C. Meng, J. L. Peng, M. Zhang, F. J. Liu, L. W. Ma and H. Wei, *ACS Appl. Polym. Mater.*, 2020, **2**, 263–272.
54 Y. P. Liu, Y. Cong, W. Ma, G. Y. Kang, C. Meng, F. J. Liu, C.-Y. Yu and H. Wei, *ACS Biomater. Sci. Eng.*, 2020, **6**, 2812–2821.
55 Y. F. Wang, H. Wei, L. P. Zheng, Z. Z. Wu, X. L. Zhang and X. S. Zhang, *ACS Macro Lett.*, 2018, **7**, 1203–1207.
56 T. W. Wang, M. J. Li, H. X. Gao and Y. Wu, *J. Colloid Interface Sci.*, 2011, **353**, 107–115.
57 R. N. Wang, S. Yang, P. P. Xiao, Y. Sun, J. Li, X. Q. Jiang and W. Wu, *Angew. Chem., Int. Ed.*, 2022, e202201390.
58 R. N. Wang, C. F. Yin, C. R. Liu, Y. Sun, P. P. Xiao, J. Li, S. Yang, W. Wu and X. Q. Jiang, *J. Am. Chem. Soc.*, 2021, **143**, 20927–20938.
59 X. F. Ji, H. W. Shao, X. H. Li, M. W. Ullah, G. W. Luo, Z. Y. Xu, L. M. Ma, X. C. He, Z. H. Lei, Q. Li, X. L. Jiang, G. Yang and Y. Zhang, *Biomaterials*, 2022, **285**, 121530.
60 J. H. Ruan, Q. L. Yu, H. M. Cui, X. Qin, L. M. Qin, S. Chen, D. C. Niu and C. Y. Fan, *Appl. Mater. Today*, 2021, **25**, 101216.
61 X. Y. Wang, H. J. Zhao, Z. C. Liu, Y. T. Wang, D. Lin, L. Chen, J. W. Dai, K. L. Lin and S. G. Shen, *Chem. Eng. J.*, 2021, **417**, 129284.
62 K. Ren, X. Ke, Z. Chen, Y. Zhao, L. He, P. Yu, J. Q. Xing, J. Luo, J. Xie and J. S. Li, *Carbohydr. Polym.*, 2021, **274**, 118672.
63 S. Brown, S. Kumar and B. Sharma, *Acta Biomater.*, 2019, **93**, 239–257.
64 M. P. J. van den Borne, N. J. H. Raijmakers, J. Vanlauwe, J. Victor, S. N. de Jong, J. Bellemans and D. B. F. Saris, *Osteoarthritis Cartilage*, 2007, **15**, 1397–1402.
65 C. Yang, Z. W. Zheng, M. R. Younis, C. L. Dong, Y. H. Chen, S. Lei, D.-Y. Zhang, J. Y. Z. Wu, X. Q. Wu, J. Lin, X. S. Wang and P. Huang, *Adv. Funct. Mater.*, 2021, 2101372.